Available online at www.sciencedirect.com

SciVerse ScienceDirect

Fusion Engineering and Design 00 (2012) 000–000

Neutron and gamma-ray transport calculations in support of the design of the radiation shielding for the TOFED neutron spectrometer at LHD

S. Sangaroon[a,b]*, K. Ogawa[a,c], M. Isobe[a,c], M. I. Kobayashi[a,c], S. Conroy[d], Y. Zhang[e], T.S. Fan[e], and M. Osakabe[a,c]

[a]*National Institute for Fusion Science, National Institutes of Natural Sciences, Toki, Japan*
[b]*Department of Physics, Faculty of Science, Mahasarakham University, Maha Sarakham, Thailand*
[c]*The Graduate University for Advanced Studies, SOKENDAI, Toki, Japan*
[d]*Department of Physics and Astronomy, Uppsala University, Uppsala, Sweden*
[e]*State Key Laboratory of Nuclear Physics and Technology, Peking University, Beijing, China*

Abstract

The neutron emission spectrometer (NES) has been commissioned at the Large Helical Device (LHD) with a new Time-Of-Flight-Enhanced-Diagnostics (TOFED). The aim of the TOFED is to measure the neutron energy spectrum to study the fast-ions behavior such as high-energy ions created by ion cyclotron resonance heating, beam ions, and D-D fusion born 1 MeV tritons in LHD. The instrument is assembled of the first detector S1 and the second detector S2. In 2019, TOFED was installed at Z =13.5 m below midplane without the radiation shielding and was initially commissioned. Due to neutrons streaming through a considerable number of holes in the LHD torus hall, the ambient background radiation at the TOFED was higher than expected, which causes the large number of coincidental events on the detectors. The obtained time difference between S1 and S2 provides the strong suggestion of TOFED relocation and of TOFED shielding development. In 2020, TOFED was relocated to the basement at Z =18.5 m below midplane. In this work, a dedicated radiation shielding design is investigated using the Monte Carlo N-Particle code (MCNP6). The shielding design fulfills the design criteria on the radiation moderation capability and engineering constraints. Due to the design criteria, borated polyethylene with thickness of 20 cm is being considered as a neutron shielding and lead with thickness of 5 cm is being considered as a gamma-ray shielding. The shielding is suggested to be a rectangular polyhedron shaped roof. With the designed shielding, neutron flux is reduced by approximately two orders of magnitude at S1 and by approximately more than two orders of magnitude at S2 while prompt gamma-ray fluence is reduced by approximately two orders of magnitude. Here, the detailed design of radiations shielding for the TOFED at LHD is presented. The appropriate radiation shielding from this work will be installed at TOFED.

Keywords: time-of-flight technique; neutron spectrometer; TOFED; LHD

1. Introduction

To sustain the high-performance plasma in fusion devices, the measurements of neutron emission from fusion plasma using comprehensive neutron diagnostics are widely employed to perform measurements of important plasma parameters, for example, energetic-particle behavior and fuel ion ratio. More detailed information such as effective energetic-ions temperature and fractional conditions of neutron emission produced from the fuel ions in the mixed D and DT plasmas are mostly obtained from the neutron emission spectrometer (NES) [1-3]. The high efficiency and powerful diagnostics are offered by the neutron Time-Of-Flight (TOF) technique [4-8]. The method is based on the measurement of the flight time of the neutrons scattered from the first detector (S1) to the second detector (S2). The S1 and S2 are placed on the constant TOF sphere with the proper

radius (L). The S1 (providing the 'start' signal) is located in a collimated neutron beam. The S2 (providing the 'stop' signal) is located in a proper position which provides the constant Time-of-Flight (t_{tof}) between S1 and S2 of the incoming neutron as: $t_{\mathrm{tof}}^2 = 2m_{\mathrm{n}}\,L^2/E_n$. The m_{n} and E_{n} are the mass and the energy of incoming neutrons, respectively. The Time-Of-Flight neutron spectrometer (the so-called TOFOR) has been operated at the Joint European Torus (JET) in order to measure 2.45 MeV neutron spectrometer from deuterium plasma at the high count rate of ~100 kHz range in different auxiliary heating scenarios [9,10]. The instrument is assembled of S1 and individual ring of S2. To increase the detection performance, the TOFOR II which is assembled of double rings of S2 has been designed [11]. Regarding the improvement of gain performance, the Time-Of-Flight-Enhanced-Diagnostics was developed in Beijing University and installed at Experimental Advanced Superconducting Tokamak (EAST) which aims to study the fuel ion during the neutral beam (NB) injection [12,13].

At the Large Helical Device (LHD), the comprehensive neutron diagnostics are developed and working in order to enhance the understanding of the energetic-particle physics in the deuterium plasma experiments [14-18]. To emphasize understanding of energetic-ions behavior, such as high-energy ions created by ion cyclotron resonance heating, beam ions, and 1 MeV tritons in LHD, the newly installed TOF spectrometer based on the design concept of Time-Of-Flight-Enhanced-Diagnostics at EAST [12] (hereafter called as TOFED) has been developed and installed at LHD [19]. During the deuterium experiments at LHD in 2019, the TOFED was initially commissioned. The preliminary results show that the background radiation at TOFED is high. This paper is devoted to discussing the shielding design for TOFED which aims to reduce the scattered neutrons and prompt gamma-rays. A dedicated radiation shielding design is investigated using the general-purpose Monte Carlo N-Particle transport code (MCNP6) [20] with the cross-section library of FENDL-3.0 [21]. This paper is organized in the following manner: the detailed information of the TOFED instrument and preliminary results from the initial commissioning in 2019 are presented in section 2. The design criteria of the radiation shielding are provided in section 3. The MCNP6 model description is provided in section 4. The obtained radiations shielding results are shown in section 5. Finally, in section 6, the summary is given.

2. TOFED instrument and initial commissioning

The TOFED spectrometer is designed to permit operation at the LHD in a few hundred kHz range. To measure a collimated neutron flux vertically from LHD plasma, the TOFED shares one of the collimators with vertical neutron camera (VNC) at major radius (R) of 3.72 m which is installed at the LHD lower port (the so-called 2.5L port) [18]. The TOFED is assembled from two fast timing plastic scintillator detector sets (S1 and S2). The S1 consists of five plastic scintillators, i.e., EJ-228 [22] intended for very fast timing applications with the diameter of 40 mm and the thickness of 6 mm each, stacked together and placed in a collimated neutron beam at R = 3.72 m. S2 is composed of two rings of fast timing plastic scintillator detectors. The upper ring of S2 (S2-upper) is composed of forty plastic scintillators, i.e., EJ-200 [23]. The scintillator of S2-upper has a dimension of ~280 mm × 70 mm and a thickness of 17 mm. The lower ring of S2 (S2-lower) is also composed of forty plastic scintillators, i.e., EJ-200. The scintillator of S2-lower has a dimension of ~235 mm × 95 mm and thickness of 17 mm. The S1 and S2 scintillators material density are 1.023 g/cm^3 with H:C atomic ratio of 1.1:1. The performance of TOFED on 2.45 MeV neutron measurement has been estimated as: the t_{tof} is centered at 69.5 ns; the Full Width at Half Maximum (FWHM) by geometry is 2.09 ns; and the expected coincidental neutron count (C_d) is 0.25 counts per neutron fluence [24].

During the LHD deuterium plasma experiment campaign in 2019, TOFED was assembled and installed on the deck, without neutron and gamma-ray shielding, at Z = 13.5 m below the midplane. Four S1 scintillators, two S2-upper scintillators, and two S2-lower scintillators were installed and operated. The relative 2.45 MeV neutron fluence at S1 (Ψ_{S1}) of 2.48 × 10^{-11} neutrons per cm^2 per emitted source neutron has been obtained using MCNP6. The obtained result of deuterium plasma shot #156489 is discussed in this work. The neutron yield (Y_{n}) measured by the neutron flux monitor (NFM) is 2.7 × 10^{14} neutrons. Based on the design performance of TOFED, the calculated coincidental 2.45 MeV neutron counts of TOFED (C_{cal}) in deuterium plasma shot #156489 would be $C_{cal} = C_d \times \Psi_{S1} \times Y_n \times (4/5) \times (2/40)$ ~67 counts, where 4/5 and 2/40 are the number of operated S1 and S2 scintillators, respectively. The obtained C_{cal} is low due to the lack of S1 and S2 scintillators of TOFED. The synthetic flight time spectrum of C_{cal} ~67 counts with the FWHM of 2.09 ns and peak centered at 69.5 ns is calculated (see Fig. 1).

The initial commissioning of TOFED was performed. The time difference (t_{S2}-t_{S1}) histogram of events which have a collision on S1 and S2 is preliminarily obtained as shown in Fig. 1. The result shows the flat histogram of events, as expected in a situation dominated by random coincidences. At the present level of statistics, no indication of a coincidence peak due to 2.45 MeV neutron, centered at t_{tof} ~69.5 ns, is observed. As is clearly seen by the calculated counts of coincidences under these circumstances (shaded peak in Fig. 1), the true coincidences are expected on a level of approximately an order of magnitude below the random background. Based on the experiment and calculation, the signal-to-background counts ratio of approximately 1:10 is given. The contributions to the experimental results could be affected by: *i*) the irreducible random coincidences due to neutron scattering in the S1 towards the S2; *ii*) an ambient background (which is the main focus of this

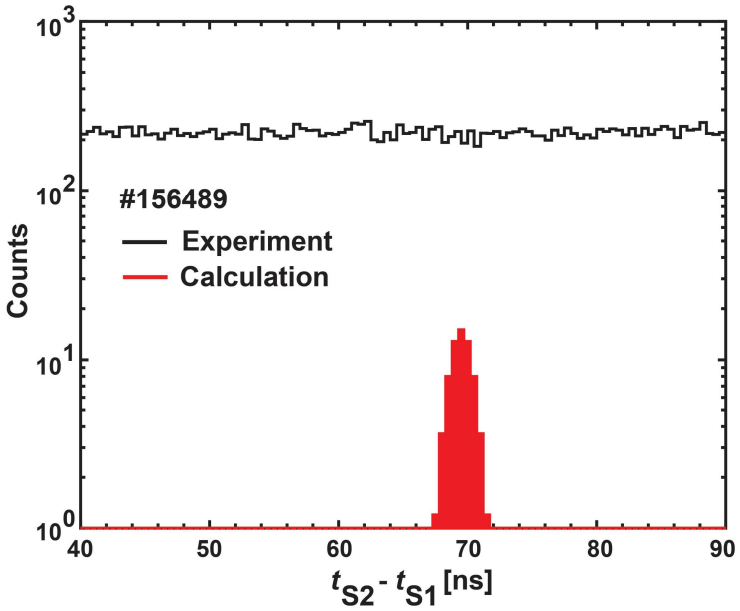

Fig. 1. The TOFED time difference histogram from the experiment and the calculation of LHD deuterium plasma shot #156489. Note that the calculation is estimated for 2.45 MeV neutrons.

paper); and *iii*) neutrons back-scattered from the concrete floor. Note that the affect from *i*) is beyond the scope of this paper. The affect from *iii*) is found to be negligible at TOFED. The ambient background radiation in *ii)* may be caused by the uncollimated neutrons, neutrons scattering in the LHD surrounding structure, and the gamma-rays. Because the detectors of the TOFED are exposed to both neutron and gamma-ray, therefore, the gamma-ray is a concern. Gamma-rays are partly emitted from the LHD plasma itself (not discussed in this paper). In addition, prompt gamma-rays are generated by the neutrons capture reaction in the LHD surrounding structures and TOFED neutron shielding (which is designed in this paper). The TOFED radiation shielding design in this work is devoted to shield the uncollimated neutrons, scattered neutrons, and the prompt gamma-rays.

In 2020, TOFED (assembled of S1 and S2) was relocated to the LHD basement at Z =18.5 m below midplane and shares one of the collimators with VNC at R = 3.72 m at 2.5L port. An additional seven S2-upper scintillators and seven S2-lower scintillators were installed. The appropriate neutron and gamma-ray shielding design in this work will be installed at TOFED.

3. Design criteria

To shield the ambient background radiations (as discussed in section 2), the radiation shielding of TOFED is designed. The design in this work is aimed to fulfill the following criteria:

1. Provide a high effectiveness as a neutron and prompt gamma-ray moderators;
2. Provide the low prompt gamma-ray generated from neutron capture reaction;
3. Fit in the available space at the LHD basement;
4. Provide the lighter-weight of material;
5. Provide the cost effectiveness of material and fabrication.

Due to a high effectiveness as a neutron moderator, the following materials were selected as a neutron shielding:

1. Borated polyethylene with 10% boron doped by weight (hereafter called as PE) has a density of 0.95 g/cm^3 (see Table 1). Due to its high hydrogen and boron content, neutrons are efficiently moderated. However, the level of 0.42 MeV gamma-ray emitted after neutron capture in boron is a concern. PE is widely used as a neutron moderator due to its light-weight and cost-effectiveness [25];
2. Hematite (Fe_2O_3)-doped heavy concrete (hereafter called as HC) has a density of 3.55 g/cm^3. It is obtained by adding high-density aggregates into ordinary concrete. It is found that the HC has a high capability of neutron and gamma-ray absorption [26];

Table 1 Neutron and gamma-ray shielding material, density, thickness, and approximate weight.

Type	Material	Thickness [cm]	Weight [tons]
Neutron shielding	Borated polyethylene $\rho = 0.95$ g/cm^3	10 20	3.98 7.11
	Hematite-doped heavy concrete $\rho = 3.55$ g/cm^3	30 50	62.19 94.83
	Ordinary concrete $\rho = 2.1$ g/cm^3	30 50	36.79 59.10
	Neutron-stop LM $\rho = 1.1$ g/cm^3	20	8.23
Gamma-ray shielding	Lead $\rho = 11.34$ g/cm^3	5 10	22.49 39.72
	Gamma-stop LA $\rho = 7.1$ g/cm^3	5 10	14.08 24.87

Table 2 Material composition of neutron-stop LM and gamma-stop LA [27]. Note that LM and LA are given by the manufacturer.

Name of material	Element	% Weight
Neutron-stop LM	H	6.5
	B	15.7
	C	30.2
	O	17.3
	Si	30.3
Gamma-stop LA	H	0.7
	C	2.8
	O	1.8
	Si	3.2
	W	91.5

3. Ordinary concrete (hereafter called as OC) has a density of 2.1 g/cm^3. OC is also widely used as a neutron and gamma-ray shielding due to its higher density compared with the PE.
4. Neutron-stop LM (hereafter called as LM) has a density of 1.1 g/cm^3. LM is a product specially designed for neutron radiation shielding (Ask Sanshin Engineering Corp. [27]). The percentage by weight of composition of LM is shown in Table 2. The LM is selected in this study due to its high effectiveness as a neutron moderator and its light-weight.

The prompt gamma-ray generated by the neutron capture reactions in the neutron shielding, especially in PE and LM, is a concern. Therefore, the lead and gamma-stop LA (Ask Sanshin Engineering Corp. [27]) were considered due to its high effectiveness as a gamma-ray moderator for the PE and LM cases. Gamma-stop LA (hereafter called as LA) is a product specially designed for gamma-ray shielding (see Table 2).

Design criteria (1) and (2) relate the signal-to-background counts ratio. For the shielding design in this work, the signal-to-background counts ratio of 10:1 is set a target value. Based on the obtained signal-to-background counts ratio value in the initial commissioning state, the reduction of background radiation of approximately two orders of magnitude is required. In design criteria (3), the inner dimension of approximately 3 m × 3 m is limited by the rectangular stainless steel base structure of TOFED. The outer diameter of less than approximately 4 m × 4 m is limited by the LHD concrete pillar (see Fig. 2) and the stairs. Note that the rectangular stainless steel base structure of TOFED and the stairs are not modelled in in this work. We set the different thicknesses of the neutron and the gamma-ray shielding due to the available space at the TOFED position. The thickness of neutron and gamma-ray shielding in this study is presented in Table 1. In order to satisfy the reduction of the ambient background radiations at the required level, PE and LM of 20 cm is required while HC and OC of up to 50 cm is required. The weight of neutron shielding is approximately calculated by the overall weight of shielding house which has inner diameter of 3 m × 3 m and has total height (rectangular polyhedron shaped roof) of 2.5 m as well as the weight of collimator with diameter of 4 cm and length of 60 cm (see Fig. 2). The weight of gamma-ray shielding is approximately calculated by the overall weight of shielding house which has outer diameter of 3 m × 3 m and has total height (rectangular polyhedron shaped roof) of approximately 2.5 m (see Fig. 2). To fulfill design criteria (3)-(5), the radiation shielding in this work is aiming for compactness, light-weight, and cost effectiveness.

4. Model description and simulations

The neutron and the prompt gamma-ray fields at TOFED are investigated using the MCNP6 with the cross-section library of FENDL-3.0. The MCNP6 model of LHD and torus hall based on the simplified computer aided design (CAD) drawing was used for three-dimensional LHD neutronics calculations [28-32]. Fig. 2(a) shows the poloidal cross section view of the LHD, torus hall, VNC, and TOFED at 2.5L port. For the VNC, parallel vertical sight lines of stainless steel (SUS304) pipes with 3 cm of inner diameter embedded in the 1.5 m thick hematite-doped heavy concrete and installed in the 2 m thick torus hall floor ordinary concrete are modeled as collimators at 2.5L port of LHD. Note that the VNC has eleven sight lines which align radially with the spatial distance of 9 cm [18]. The TOFED field of view is adjusted by one collimator of VNC at R = 3.72 m. TOFED equipped with the S1, S2, and stainless steel rings is modelled in the LHD basement at Z =18.5 m below midplane.

Firstly, the single layer of neutron shielding made of different materials and thicknesses (see Table 1) are modelled (hereafter called as: PE = 10 cm, PE = 20 cm, HC = 30 cm, HC = 50 cm, OC = 30 cm, OC = 50 cm, and LM = 20 cm). The neutron flux and the prompt gamma-ray fluence at S1 and S2 are obtained. Secondly, the inner layer (see Fig. 2(b) and 2(c)) made of different materials and thicknesses (see Table 1) are modelled as a gamma-ray shielding (hereafter called as: lead = 5 cm, lead = 10 cm, LA = 5 cm, and LA = 10 cm) for PE = 10 cm, PE = 20 cm, and LM = 20 cm cases. The prompt gamma-ray fluence at S1 is obtained.

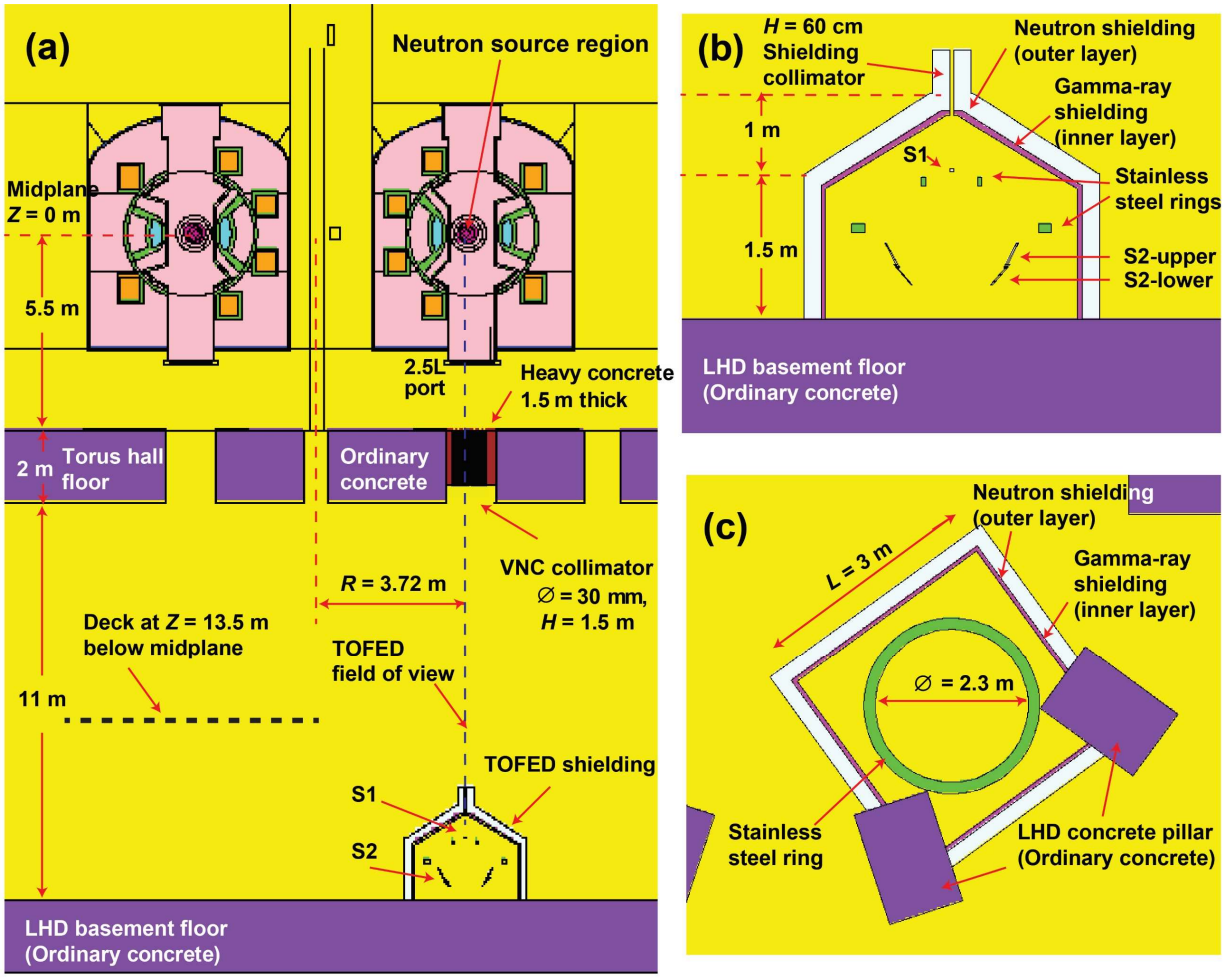

Fig. 2. The MCNP6 calculation model of: (a) poloidal cross-section view of LHD, torus hall, VNC, and TOFED at 2.5L port; (b) poloidal cross-section view of the TOFED shielding house whereas, for example, the outer layer is neutron shielding made of 20 cm of borated polyethylene (white) and the inner layer is gamma-ray shielding made of 5 cm of lead (magenta); and (c) the top view of the TOFED detector holder made of stainless steel ring (green) and shielding house (white and magenta).

In order to study the capabilities of the shielding, a point neutron source and a toroidal neutron source have been modelled. In the case of point neutron source, the virgin neutron energy is set to be 2.45 MeV and is placed on the torus midplane at collimator central axis of $R = 3.72$ m. In the case of toroidal neutron source, a uniform toroidal and poloidal symmetry, donut-shaped, neutron source with the diameter of 60 cm in poloidal view centered on the torus midplane is modelled. The virgin neutron energy is assumed to be 99.5% and 0.5% of 2.45 MeV and 14.1 MeV, respectively [14,33]. The maximum total neutron emission rate (S_n) in LHD is expected to be 1.9×10^{16} n/s [34]. The neutron and the gamma-ray fluences at S1 and S2 have been calculated by track length estimation tally (the so-called cell tally in MCNP6). The simulation was performed by 10^9 neutron histories. The weight window variance reduction method is used. To satisfy the design criteria, the optimization with different materials and thicknesses of the neutron and the gamma-ray shielding is aimed at reductions of the ambient background radiations of approximately two orders of magnitude.

5. Results

5.1. Neutron shielding results for point neutron source

Fig. 3(a) shows an example of the neutron spectra at S1 and S2 in energy range of 0.1-2.45 MeV. Without neutron and gamma-ray shielding (hereafter called as w/o n-γ shielding), neutron spectrum at S1 shows a clear peak of virgin neutron at the energy of 2.45 MeV whereas the contributions of scattered neutrons in energy range of 0.1-2.4 MeV are approximately two orders of magnitude lower than virgin neutron. The neutron flux at S1 is dominated by approximately 77% of virgin 2.45 MeV neutrons. The obtained results show that the neutron spectra at S2, which is placed outside the neutron beam, are mainly dominated by the scattered neutrons for all cases, e.g., w/o n-γ shielding, PE = 20 cm, HC = 50 cm, and LM = 20 cm. At S2, in the case of w/o n-γ shielding, the scattered neutron energy distribution in energy range of 0.1-2.4 MeV is between ~10^4 - 10^6 n/cm^2/s/MeV. In the case of PE = 20 cm, HC = 50 cm, and LM = 20 cm, the scattered neutron energy distribution at S2 is ~10^4 n/cm^2/s/MeV and is three orders of magnitude lower than the scattered neutron flux observed at S1. The results show that the neutrons observed at S1 are mainly dominated by virgin neutron while the neurons observed at S2 are mainly dominated by scattered neutron.

The total neutron fluxes at S1 and S2 are obtained and presented in Fig. 3(b). Since S1 is placed in collimated neutron beam and the point neutron source is located at a central axis of TOFED field of view, the total neutron flux at S1 is constant in all cases. At S2, the total neutron flux of ~10^7 n/cm^2/s is obtained in the case of the w/o n-γ shielding. When the neutron shielding is used, the total neutron flux at S2 is reduced by approximately two orders of magnitude. The obtained results show

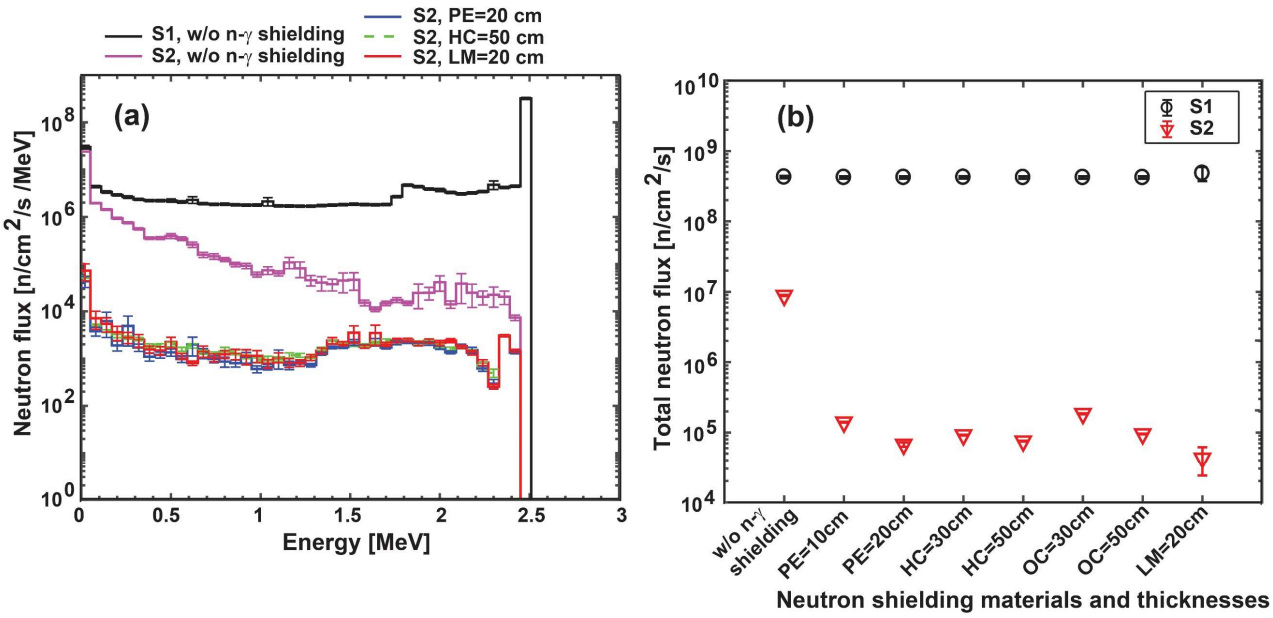

Fig. 3. (a) An example of neutron spectra at S1 and S2. (b) The total neutron fluxes at S1 and S2 for different neutron shielding materials and thicknesses.

that the neutrons are well collimated through the collimator to S1. In addition, all cases of neutron shielding in this study have a high effectiveness in shielding the scattered neutron at S2.

5.2. Neutron shielding results for toroidal neutron source

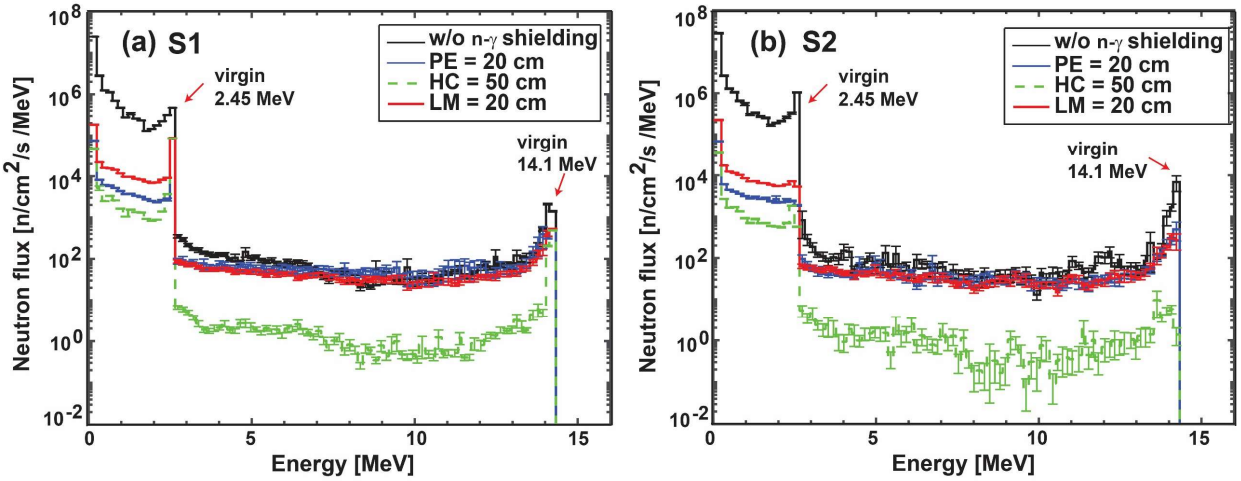

Fig. 4. An example of neutron energy spectra at (a) S1 and (b) S2 for different neutron shielding materials and thicknesses.

Fig. 4(a) shows an example of neutron spectra in energy range of 0.1-14.1 MeV at S1. In the case of w/o n-γ shielding, the level of scattered neutrons dominated in the neutron spectrum is high. When the neutron shielding is used, i.e., PE = 20 cm, HC = 50 cm, and LM = 20 cm, the contribution of scattered neutrons at energy below 2.45 MeV is significantly reduced by approximately two orders of magnitude. Fig. 4(b) shows an example of neutron spectra in energy range of 0.1-14.1 MeV at S2. In the case of w/o n-γ shielding, a clear peak of virgin neutron at energy of 2.45 MeV is obtained at S2 due to its larger volume of scintillator to observe neutron than the volume of S1. When the neutron shielding is used, i.e., PE = 20 cm, HC = 50 cm, and LM = 20 cm, no peaks of virgin neutron 2.45 MeV and virgin neutron 14.1 MeV are observed. Similar to the results on S1, when the neutron shielding is used the contribution of scattered neutron at energy below 2.45 MeV is significantly reduced. The obtained results at S1 and S2 show that the scattered neutrons in energy range of 2.45 MeV < E_n < 14.1 MeV are significantly reduced by approximately two orders of magnitude by using HC = 50 cm. The PE = 20 cm and the LM = 20 cm are ineffectiveness in shielding neutrons in energy range of 2.45 MeV < E_n < 14.1 MeV.

The percentage of DD virgin neutron and DT virgin neutron at S1 are calculated by the ratio of 2.45 MeV virgin neutron flux and of 14.1 MeV virgin neutron flux, respectively, to total neutron flux. The percentage virgin neutron shows in Fig. 5(a). In the case of w/o n-γ shielding, ~5.28% of DD virgin neutron and ~0.01% of DT virgin neutron are observed. When the neutron shielding is used, the percentages of DD virgin neutron and DT virgin neutron increase significantly. The percentages of DD virgin neutron increase to 74.58%, 57.82%, and 35.38% by using HC = 50 cm, PE = 20 cm, and LM = 20 cm, respectively. The percentages of DT virgin neutron increase to 0.42%, 0.34%, and 0.21% by using HC= 50 cm, PE = 20 cm and LM = 20 cm, respectively. Less than 35% and less than 0.2% of DD virgin neutron and DT virgin neutron, respectively, are obtained when PE = 10 cm, HC = 30 cm, OC = 30 cm, and OC = 50 cm are used. The obtained results show that the HC = 50 cm, PE = 20 cm, and LM = 20 cm have a high effectiveness in shielding the scattered neutrons and provide the high level of the virgin neutron fluxes at S1.

Fig. 5(b) shows integrated neutron fluxes over the energy range of 0.1-14.1 MeV at S1 and S2. The obtained results at S1 show that total neutron fluxes are reduced less than two orders of magnitude by using PE = 10 cm, HC = 30 cm, OC = 30 cm, OC = 50 cm, and LM = 20 cm, and are reduced by approximately two orders of magnitude by using PE = 20 cm and HC = 50 cm. The obtained results at S2 show that total neutron fluxes are reduced less than two orders of magnitude by using PE = 10 cm and OC = 30 cm and are reduced approximately two orders of magnitude by using HC = 30 cm, OC = 50 cm, and LM = 20 cm. Total neutron fluxes at S2 are reduced more than two orders of magnitude by using PE = 20 cm and HC = 50 cm. Even though the HC = 30 cm and OC = 50 cm provide the low background neutron fluxes and satisfy the design criteria but the obtained DD virgin neutron and DT virgin neutron to total neutron (Fig. 5(a)) is relatively low. The results show that the

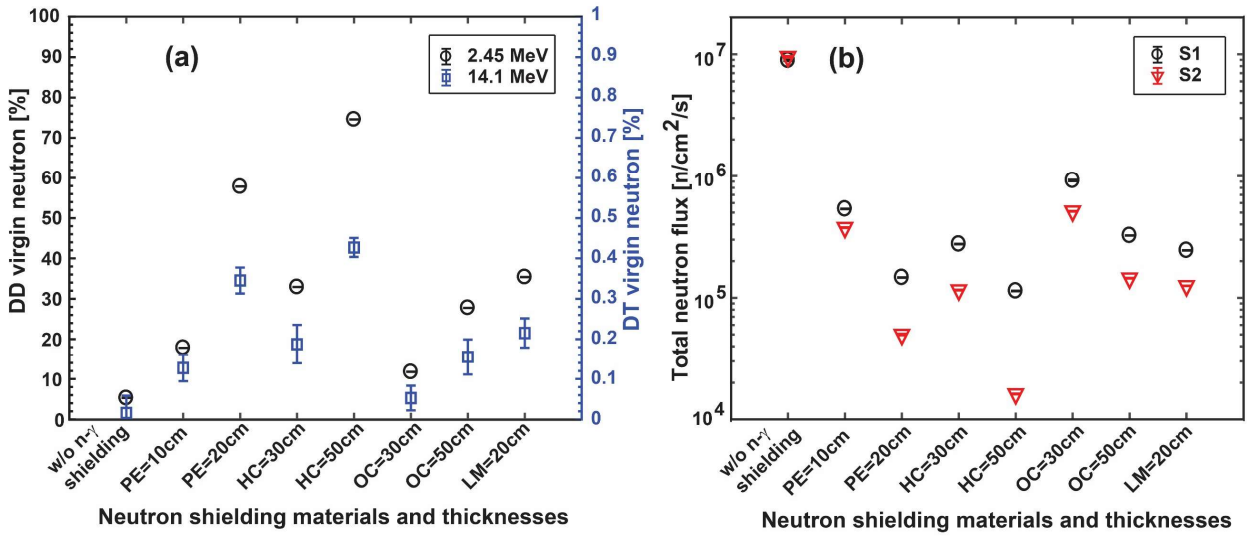

Fig. 5. (a) The percentage of virgin neutron energy of 2.45 MeV (left axis) and of virgin neutron energy of 14.1 MeV (right axis) to total neutron flux at S1. (b) The total neutron fluxes at S1 and S2 for different neutron shielding materials and thicknesses.

HC = 50 cm has a high effectiveness in shielding the neutron flux in order to satisfy the requirement of TOFED but HC = 50 cm provides the heavy-weight shielding of ~94 tons (see Table 1). On account of the engineering and design constraints, the light-weight shielding made of PE = 20 cm (weight of ~7 tons) or made of LM = 20 cm (weight of ~8 tons) is considered.

5.3. Gamma-ray shielding results for toroidal neutron source

Here, the relative prompt gamma-ray fluence per emitted source neutron generated from the neutron capture in the LHD surrounding structure and in the neutron shielding is obtained. Fig. 6 shows the prompt gamma-ray spectra in energy range of ~0.05-10 MeV obtained at S1. In the case of w/o n-γ shielding, the level of relative prompt gamma-ray fluence is approximately 10^{-12} γ-rays per cm^2 per emitted source neutron. It is clearly seen that the prompt gamma-ray fluence is significantly moderated by the HC = 50 cm. The PE = 20 cm is effective in shielding the prompt gamma-ray in energy range of above 0.42 MeV to 6 MeV. Nevertheless, the prompt gamma-ray, i.e., ~0.42 MeV is generated in the PE. Here, in the case of neutron shielding, i.e., PE and LM, the different thicknesses of lead and LA are considered and modelled as gamma-ray shielding. It is found that the prompt gamma-ray fluence is significantly reduced when the PE = 20 cm with lead = 5 cm or LM = 20 cm with LA = 10 cm is used.

Fig. 7 shows the integrated prompt gamma-ray fluence, which has energy above 0.1 MeV. The results show that, HC and OC provide a low level of prompt gamma-ray fluences at S1 due to the high effectiveness in shielding the ambient gamma-rays and low generated prompt gamma-ray from the neutron capture reaction. Nevertheless, HC and OC provide the heavy-weight shielding (see Table 1). The obtained total prompt gamma-ray fluences are high when the PE or the LM is used due to the emitted of the prompt gamma-ray from neutron capture reactions in the PE and LM. Therefore, the lead or the LA is used. The total prompt gamma-ray fluence is reduced by nearly two orders of magnitude when the PE = 20 cm with lead = 5 cm is used. On account of the design criteria, the PE = 20 cm is being considered as a neutron shielding due to a high effectiveness in shielding neutron, lighter-weight, and cost effectiveness compared with the LM = 20 cm. The lead = 5 cm is being considered as a gamma-ray shielding due to a high effectiveness in shielding gamma-ray, lighter-weight compared with lead = 10 cm, and cost effectiveness compared with the LA = 10 cm. The overall weight of the neutron and the gamma-ray shielding is approximately 30 tons.

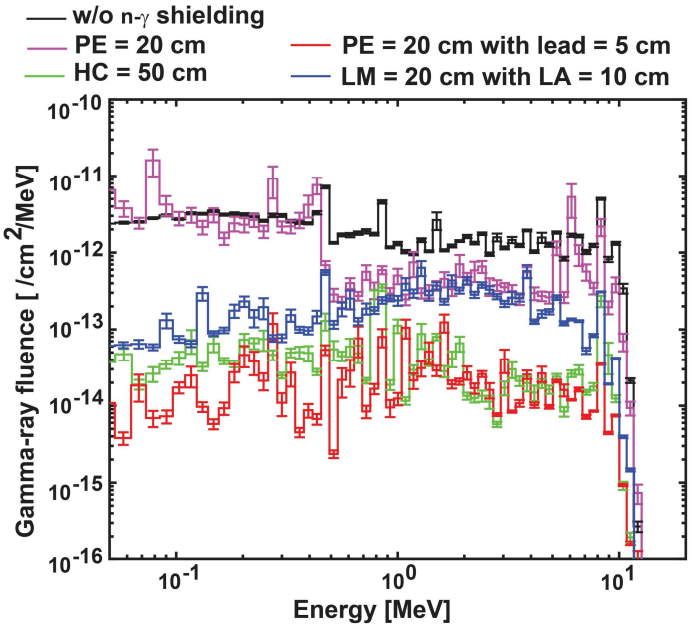

Fig. 6. An example of prompt gamma-ray spectra at S1 for different neutron and gamma-ray shielding materials and thicknesses. Note that the prompt gamma-ray fluence in this figure is presented in relative value per emitted source neutron.

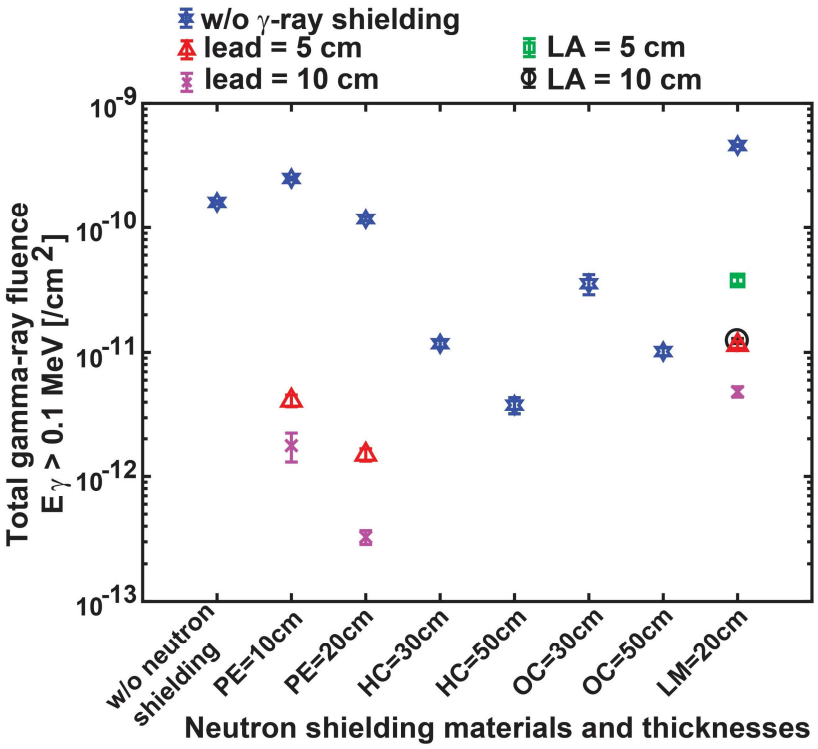

Fig. 7. Total prompt gamma-ray fluence at S1 for different neutron and gamma-ray shielding materials and thicknesses. Note that the prompt gamma-ray fluence in this figure is presented in relative value per emitted source neutron.

6. Summary

The obtained results from the initial commissioning during the LHD deuterium experiment campaign in 2019 provide the strong suggestion of TOFED shielding development at LHD. This paper is dedicated to the neutron and the gamma-ray transport calculations in support of the design of the radiation shielding for the TOFED neutron spectrometer at LHD. The optimization of materials and thicknesses were established using the MCNP6. On account of design criteria, the 20 cm of borated polyethylene is being considered for TOFED installation as a neutron shielding. The 5 cm of lead is being considered for TOFED installation as a gamma-ray shielding. The shielding house is suggested to be a rectangular polyhedron shaped roof with inner dimension of 3 m × 3 m and height of 2.5 m, approximately. The collimator, inner diameter of 4 cm, outer diameter of 44 cm, and length of 60 cm, is embedded on the top of shielding house to moderated neutron from unwanted channels of VNC. The inner layer is gamma-ray shielding and the outer layer is neutron shielding. The shielding design in this work provides a compactness, light-weight, cost effectiveness, and fit to available space in the LHD basement. The obtained results show that the neutrons are well collimated through the VNC collimator and through the TOFED collimator toward S1. Ambient background radiations are attenuated by the appropriate thickness of the TOFED shielding. The neutron shielding allows reduction of neutron flux at S1 by approximately two orders of magnitude and at S2 by approximately more than two orders of magnitude. The gamma-ray shielding allows reduction of prompt gamma-ray fluence by approximately two orders of magnitude.

Acknowledgements

This research was supported by international collaborations with overseas laboratories (UFEX105), by the NIFS Collaboration Research Program (KOAH037), by the Japan-China Post-Core-University-Program called Post-CUP (KEJC001), and by the NINS Program of Promoting Research by Networking among Institutions (Grant Number 01411702).

References

[1] O. N. Jarvis (2002). “Neutron spectrometry at JET (1983–1999)”, Nuclear Instruments and Methods in Physics Research A **476**, 474–484, https://doi.org/10.1016/S0168-9002(01)01493-0
[2] G. Ericsson (2019). “Advanced Neutron Spectroscopy in Fusion Research”, Journal of Fusion Energy **38**, 330-355, https://doi.org/10.1007/s10894-019-00213-9
[3] L. Giacomelli, A. Hjalmarsson, H. Sjöstrand, W. Glasser, J. Källne, S. Conroy, G. Ericsson, M. Gatu Johnson, G. Gorini, H. Henriksson, S. Popovichev, E. Ronchi, J. Sousa, E. Sundén Andersson, M. Tardocchi, J. Thun, M. Weiszflog and Contributors to the JET-EFDA Workprogram (2005). “Advanced neutron diagnostics for JET and ITER fusion experiments”, Nuclear Fusion **45**, 1191-1201, https://doi.org/10.1088/0029-5515/45/9/019
[4] T. Elevant, D. Aronsson, P. van Belle, G. Grosshoeg, M. Hoek, M. Olsson and G. Sadler (1991). “The JET neutron time-of-flight spectrometer”, Nuclear Instruments and Methods in Physics Research A **306**, 331–342, https://doi.org/10.1016/0168-9002(91)90340-V
[5] T. Elevant, P. van Belle, O. N. Jarvis and G. Sadler (1995). “Measurements of fusion neutron energy spectra at JET by means of time-of-flight techniques”, Nuclear Instruments and Methods in Physics Research A **364**, 333–341, https://doi.org/10.1016/0168-9002(95)00346-0
[6] G. Gorini and J. Källne (1992). “High count rate time ‐ of ‐ flight spectrometer for DD fusion neutrons”, Review of Scientific Instruments **63**, 4548-4550, https://doi.org/10.1063/1.1143663
[7] J. Källne and G. Gorini (1993). “Count rate performance of spectrometers for fusion neutrons”, Review of Scientific Instruments **64**, 2765-2770, https://doi.org/10.1063/1.1144415
[8] A. Hjalmarsson, S. Conroy, G. Ericsson, H. Henriksson, J. Källne, J. Thun and G. Gorini (2001). “Neutron time-of-flight spectrometer for high rate diagnosis of deuterium plasmas”, Review of Scientific Instruments **72**, 841, https://doi.org/10.1063/1.1321000
[9] M. Gatu Johnson, L. Giacomelli, A. Hjalmarsson, M. Weiszflog, E. Andersson Sundén, S. Conroy, G. Ericsson, C. Hellesen, J. Källne, E. Ronchi, H. Sjöstrand, G. Gorini, M. Tardocchi, A. Murari, S. Popovichev, J. Sousa, R. C. Pereira, A. Combo, N. Cruz and JET EFDA Contributors (2006). “The TOFOR neutron spectrometer and its first use at JET”, Review of Scientific Instruments **77**, 10E702, https://doi.org/10.1063/1.2219422
[10] M. Gatu Johnson, L. Giacomelli, A. Hjalmarsson, J. Källne, M. Weiszflog, E. Andersson Sundén, S. Conroy, G. Ericsson, C. Hellesen, E. Ronchi, H. Sjöstrand, G. Gorini, M. Tardocchi, A. Combo, N. Cruz, J. Sousa and S. Popovichev (2008). “The 2.5-MeV neutron time-of-flight spectrometer TOFOR for experiments at JET”, Nuclear Instruments and Methods in Physics Research Section A **591**, 417-430, https://doi.org/10.1016/j.nima.2008.03.010
[11] X. Zhang, J. Källne, G. Gorini, M. Nocente, T. Fan, X. Yuan, X. Xie and Z. Chen (2014). “Second generation fusion neutron time-of-flight spectrometer at optimized rate for fully digital data acquisition”, Review of Scientific Instruments **85**, 043503, https://doi.org/10.1063/1.4869804
[12] X. Zhang, Z. Chen, X. Peng, Z. Hu, T. Du, Z. Cui, X. Xie, X. Yuan, T. Fan, J. Kallne, G. Gorini, M. Nocente, M. Tardocchi, L. Hu, G. Zhong, S. Lin, B. Wan, X. Li, G. Zhang and J. Chen (2014). “Diagnosing NB plasmas on the EAST tokamak with new time-of-flight neutron spectrometer”, Nuclear Fusion **54**, 104008, https://doi.org/10.1088/0029-5515/54/10/104008
[13] T. F. Du, Z. J. Chen, X. Y. Peng, X. Yuan, X. Zhang, G. Gorini, M. Nocente, M. Tardocchi, Z. M. Hu, Z. Q. Cui, X. F. Xie, L. J. Ge, L. Q. Hu, G. Q. Zhong, S. Y. Lin, B. N. Wan, X. Q. Li, G. H. Zhang, J. X. Chen and T. S. Fan (2014). “Design of the radiation shielding for the time of flight enhanced diagnostics neutron spectrometer at Experimental Advanced Superconducting Tokamak”, Review of Scientific Instruments **85**, 11E115,

https://doi.org/10.1063/1.4891059
[14] M. Isobe, K. Ogawa, T.Nishitani, N. Pu, H. Kawase, R. Seki, H. Nuga, E. Takada, S.Murakami, Y. Suzuki, M.Yokoyama, M. Osakabe and LHD Experiment Group (2018). "Fusion neutron production with deuterium neutral beam injection and enhancement of energetic-particle physics study in the large helical device", Nuclear Fusion **58**, 082004, https://doi.org/10.1088/1741-4326/aabcf4
[15] K. Ogawa, M. Isobe, T. Nishitani, S. Murakami, R. Seki, H. Nuga, S. Kamio, Y. Fujiwara, H. Yamaguchi, Y. Saito, S. Maeta, M. Osakabe and LHD Experiment Group (2019). "Energetic ion confinement studies using comprehensive neutron diagnostics in the Large Helical Device", Nuclear Fusion **59**, 076017, https://doi.org/10.1088/1741-4326/ab14bc
[16] M. Isobe, K. Ogawa, T. Nishitani, H. Miyake, T. Kobuchi, N. Pu, H. Kawase, E. Takada, T. Tanaka, S. Li, S. Yoshihashi, A. Uritani, J. Jo, S. Murakami, M. Osakabe, and LHD Experiment Group (2018). "Neutron diagnostics in the Large Helical Device", IEEE Transactions on Plasma Science **46**, 6, http://doi.org/10.1109/TPS.2018.2836987
[17] K. Ogawa, M. Isobe, E. Takada, Y. Uchida, K. Ochiai, H. Tomita, A. Uritani, T. Kobuchi, and Y. Takeiri (2014). "Progress in development of the neutron profile monitor for the large helical device", Review of Scientific Instruments **85**, 11E110, https://doi.org/10.1063/1.4890399
[18] K. Ogawa, M. Isobe, T. Nishitani, and T. Kobuchi (2018). "The large helical device vertical neutron camera operating in the MHz counting rate range", Review of Scientific Instruments **89**, 113509, https://doi.org/10.1063/1.5054818
[19] M. Isobe, K. Ogawa *et al.*, "Overview of the LHD Neutron Diagnostics", Collected papers at the 2019 Post-CUP Workshop & JSPS-CAS Bilateral Joint Research Projects Workshop 24th-26th July, 2019, Nagoya, Japan, NIFS-PROC-116. pp38-43. https://www.nifs.ac.jp/report/nifs_proc_116.pdf
[20] D. B. Pelowits (2013). "MCNP6 User's Manual", LA-CP-13-00634, Los Alamos National Laboratory. https://mcnp.lanl.gov/mcnp_manual.shtml
[21] M. B. Chadwick, et al. (2011). "ENDF/B-VII.1 Nuclear data for science and technology: Cross sections, covariances, fission product yields and decay data", Nuclear Data Sheets **112**, 2887-2996, https://doi.org/10.1016/j.nds.2011.11.002
[22] See https://eljentechnology.com/products/plastic-scintillators/ej-228-ej-230 for the specification of plastic scintillator, EJ-228.
[23] See https://eljentechnology.com/products/plastic-scintillators/ej-200-ej-204-ej-208-ej-212 for the specification of plastic scintillator, EJ-200.
[24] Lijian Ge *et al.*, Peking University (2019). "Velocity-space sensitivities of neutron emission spectrometers at EAST tokamak", private communication.
[25] see https://marshield.com/borated-polyethylene-neutron-shielding for the specification of borated polyethylene.
[26] B Aygün (2019). "Neutron and gamma radiation shielding properties of high-temperature-resistant heavy concretes including chromite and wolframite", Journal of Radiation Research and Applied Sciences **12**, 352-359, 10.1080/16878507.2019.1672312
[27] See http://www.askcorp.co.jp/pdf/material.pdf for the specification of neutron-stop LM and gamma-stop LA.
[28] T. Nishitani, K. Ogawa, M. Isobe (2017). "Monte Carlo simulation of the neutron measurement for the Large Helical Device deuterium experiments", Fusion Engineering and Design **123**, 1020–1024, https://doi.org/10.1016/j.fusengdes.2017.02.038
[29] H. Kawase, K. Ogawa, T.Nishitani, N. Pu, M. Isobe and LHD Experiment Group (2019). "Evaluation of spatial resolution of neutron profile monitor in LHD", IEEE Transactions on Plasma Science **47**, 1, https://doi.org/10.1109/TPS.2018.2876170
[30] T. Nishitani, K. Ogawa, H. Kawase, N. Pu, T. Ozaki and M. Isobe (2019). "Monte Carlo calculation of the neutron and gamma-ray distributions inside the LHD experimental building and shielding design for diagnostics", Progress in Nuclear Science and Technology **6**, 48-51, http://doi.org/10.15669/pnst.6.48
[31] T. Nishitani, K. Ogawa, K. Nishimura and M. Isobe (2016). "Radiation field estimation for the diagnostic and control components by Monte Carlo neutronics calculations with LHD 3-dimensional modeling", Plasma and Fusion Research **11**, 2405057, https://doi.org/10.1585/pfr.11.2405057
[32] S. Sangaroon, K. Ogawa, M. Isobe, M. I. Kobayashi, Y. Fujiwara, S. Kamio, R. Seki, H. Nuga, H. Yamaguchi, M. Osakabe (2020). "Performance of the newly installed vertical neutron cameras for low neutron yield discharges in the Large Helical Device", Review of Scientific Instruments **91**, 083505, https://doi.org/10.1063/5.0010302
[33] M. Isobe, H. Yamanishi, M. Osakabe, H. Miyake, H. Tomita, K. Watanabe, H. Iwai, Y. Nomura, N. Nishio, K. Ishii, J. H. Kaneko, J. Kawarabayashi, E. Takada, A. Uritani, M. Sasao, T. Iguchi, Y. Takeiri, and H. Yamada (2010). "Fusion product diagnostics planned for Large Helical Device deuterium experiment", Review of Scientific Instruments **81**, 10D310, https://doi.org/10.1063/1.3492383
[34] M. Osakabe, Y. Takeiri, T. Morisaki et. al. (2017). "Current Status of Large Helical Device and its prospect for deuterium experiment", Fusion Science and Technology **72**, 199-210, https://doi.org/10.1080/15361055.2017.1335145